

Post-print version:

METHODOLOGY FOR DROOP CONTROL DYNAMIC ANALYSIS OF MULTITERMINAL VSC-HVDC GRIDS FOR OFFSHORE WIND FARMS

E. Prieto-Araujo and F.D. Bianchi and A. Junyent-Ferre and O. Gomis-Bellmunt

This work has been published in **IEEE Transactions on Power Delivery**:

E. Prieto-Araujo and F.D. Bianchi and A. Junyent-Ferre and O. Gomis-Bellmunt, "Methodology for Droop Control Dynamic Analysis of Multiterminal VSC-HVDC Grids for Offshore Wind Farms", *IEEE Transactions on Power Delivery*, vol. 26, no. 4, pp. 2476-2485, 2011.

Final version available at:

URL: <http://ieeexplore.ieee.org/xpl/articleDetails.jsp?arnumber=5776724>

DOI: [10.1109/TPWRD.2011.2144625](https://doi.org/10.1109/TPWRD.2011.2144625)

© 2011 IEEE. Personal use of this material is permitted. Permission from IEEE must be obtained for all other users, including reprinting/republishing this material for advertising or promotional purposes, creating new collective works for resale or redistribution to servers or lists, or reuse of any copyrighted components of this work in other works.

BibTex:

```
@Article{Prieto-Araujo2011,
  Title = {Methodology for Droop Control Dynamic Analysis of Multiterminal
    VSC-HVDC Grids for Offshore Wind Farms},
  Author = {Eduardo Prieto-Araujo and Fernando D. Bianchi and Adriá Junyent
    Ferre and Oriol Gomis-Bellmunt},
  Journal = {IEEE Transactions on Power Delivery},
  Year = {2011},
  Number = {4},
  Pages = {2476-2485},
  Volume = {26},
  Doi = {10.1109/TPWRD.2011.2144625}
}
```

Methodology for droop control dynamic analysis of multi-terminal VSC-HVDC grids for offshore wind farms

Eduardo Prieto-Araujo, Fernando D. Bianchi, Adrià Junyent-Ferré, *Student Member, IEEE* Oriol Gomis-Bellmunt, *Member, IEEE*

Abstract—The article addresses the control of multi-terminal voltage source converters (VSC) at high voltage direct current (HVDC) in the context of offshore wind farms. Droop control is commonly used to regulate the DC voltage in this kind of grids, droop parameters are selected on the basis of steady-state analyses. Here, a control design methodology is proposed based on the frequency response analysis. This methodology provides a criterion to select the droop gains taking into account the performance specifications, *i.e.*, the desired voltage errors and the maximum control inputs (currents). The application of the methodology is illustrated with a four-terminal grid.

Index Terms—Offshore wind power, multi-terminal, droop control, HVDC.

I. INTRODUCTION

Nowadays, there is an increasing number of offshore wind farms. In these offshore facilities, turbines can be located tens or hundreds of kilometers away from the coast and connected to the main power grid by submarine cables. In these situations, studies have proved that the most convenient power transmission systems are the High Voltage Direct Current (HVDC) networks [1]. These grids consist of two or more converters connected to a common DC grid [2]. The most common technology in the last years has been the Line Commuted Converters (LCC) [3]. However, there is a growing trend towards the use of Voltage Source Converters (VSC) in offshore HVDC grids [1, 4, 5]. These power converters offer more possibilities for the operation of the offshore wind farms. VSC-HVDCs permit the independent control of active and reactive power and a continuous AC voltage regulation. They present no commutation failure, black-start capability, and there is no need of voltage polarity reversal to reverse power. As additional advantages, the filters are more compact and the cables lighter [6, 7]. On the other hand, the costs and the commutation losses are higher and they are able to handle only limited levels of voltage and power. The first HVDC using VSC technology in wind farms, named BorWin1, has

been commissioned in 2010 in Germany. A total of 80 wind turbines of 5 MW each are connected by 75 km underground cable and 125 km submarine cable at ± 150 kV [8].

In the near future, there will be a large amount of offshore wind farms connected with VSC-HVDC. It seems reasonable to devise offshore VSC-HVDC grids interfacing a number of such different terminals with different AC grids, resulting in the so-called multiterminal VSC-HVDC system. Multiterminal VSC-HVDC stands as an interesting solution to connect efficiently a number of offshore wind farms, but also implies several technical challenges that will have to be addressed, including control [9], operation [7] and protection [6] issues. The first multi-terminal using LCC-HVDC technology goes back to 1960s [10, 11]. It was not until 2003 that the use of multi-terminal VSC-HVDC in the aggregation of offshore wind power was proposed by Lu and Ooi [12]. A detailed analysis of different system topologies can be found in [6]. Important projects involving HVDC multi-terminal transmission are currently under study, such as the Desertec project [13] and the European offshore Supergrid [14].

The stability of AC power systems has been widely discussed in the literature, see for example [15, 16]. These studies also include HVDC systems and their possible contribution to improve AC system stability. Some DC grid management strategies based on coordinated closed-loop DC voltage control and DC droop characteristics were proposed and simulated in [17]. Liang et al. [9] addressed the modeling and simulation of multi-terminal VSC-HVDC transmissions for offshore wind power. However, to the best of our knowledge, there is no stability analysis nor systematic control design procedure for multi-terminal VSC-HVDC grids connecting offshore wind farms to AC systems. This paper investigates the stability and the dynamic behavior of multi-terminal HVDC grids in offshore wind farms applications. A design methodology of proportional control of the DC voltage based on frequency response analysis is proposed.

The paper is organized as follows. The next section provides a brief discussion of the control of VSC-HVDC multi-terminal networks. Section III presents the main contribution, a modelling procedure for complex VSC-HVDC multi-terminal systems and a methodology for the selection of the droop constant. The application of the proposed procedure is illustrated in the case of a four-terminal grid in Section IV. Finally, in Section V, some conclusion remarks are drawn.

E. Prieto-Araujo, A. Junyent-Ferré and O. Gomis-Bellmunt are with the Centre d'Innovació Tecnològica en Convertidors Estàtics i Accionaments (CITCEA-UPC), Departament d'Enginyeria Elèctrica, Universitat Politècnica de Catalunya. ETS d'Enginyeria Industrial de Barcelona, Av. Diagonal, 647, Pl. 2. 08028 Barcelona, Spain. Tel: +34 934016727, Fax: +34 934017433, e-mail: eduardo.prieto-araujo@citcea.upc.edu.

F.D. Bianchi and O. Gomis-Bellmunt are with the Catalonia Institute for Energy Research (IREC), Power Electronics and Electric Power Grids Dept., Josep Pla, B2, 08019 Barcelona, Spain.

This work was supported by the *Ministerio de Ciencia e Innovación* under the project ENE2009-08555.

II. MULTI-TERMINAL GRID CONTROL

Figure 1 illustrates a typical multi-terminal HVDC network. It consists of the DC grid, the main AC grid (or AC grids), the wind farm grids, the wind farm converters (WFCs) and the AC grid side converters (GSCs). The multi-terminal HVDC network permits the transfer of power among the different units, where the WFCs act as power sources and the GSC as loads. In this power transmission scheme, the sources inject all the available power into the grid whereas the control of the GSCs seek to maintain the DC voltage. This also includes the power sharing among the different GSCs. The normal operation may be altered when some of the converters reach the current limits. This usually occurs during severe voltage faults in the AC grid. Under these circumstances, the WFCs enter in voltage regulation mode and the GSCs extract the maximum power possible without regulating the DC voltage. In both operation modes, some converters seek to maintain the DC voltage and the others inject or extract power without controlling the voltage [7].

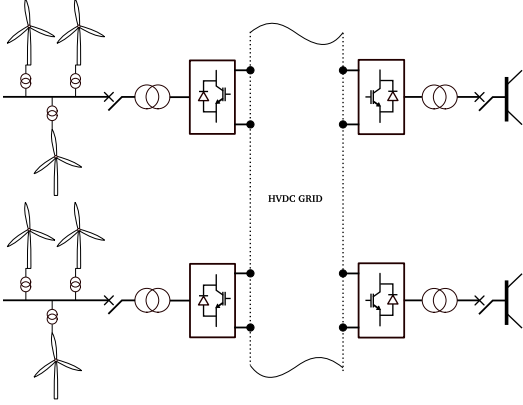


Figure 1. Typical HVDC multi-terminal network

To regulate the DC voltage, it is employed the so-called droop control, which is a technique that allows the power distribution among different terminal without communications. The control of each converter is usually implemented in two levels, an inner loop controlling the currents and an outer loop regulating the DC voltage. The droop control acts on the outer loop imposing a current reference i^* to the inner loop. The current and thus the power in the converter is directly governed by the current control in accordance with the reference imposed by the voltage loop. This control scheme is shown in Figure 2. The control law is given by the following expression

$$i^* = K_{\text{droop}}(E - E_0), \quad (1)$$

where E is the DC voltage, E_0 is the reference and K_{droop} is the droop gain. For the present study, the dynamics of current loop can be considered much faster than the outer loop. Therefore, the DC current i flowing through the converter will be assumed to be equal to the reference i^* .

The selection of the gain K_{droop} for each converter must be done taking into account the entire multi-terminal behavior. In addition to the static consideration associated to the distribution of the power sources and sinks, each local controller

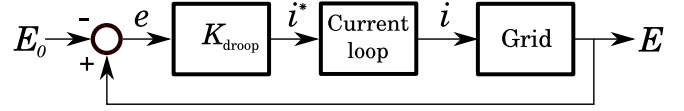


Figure 2. Droop control scheme of a VSC

can affect the global stability and the DC voltage in other terminal. For these reasons, the droop constant selection must be addressed in the context of multi-variable system theory.

III. FREQUENCY RESPONSE ANALYSIS FOR DROOP GAIN SELECTION

In this section, a methodology for the droop constant selection based on multi-variable frequency response analysis is presented. Previous to propose this methodology, it is introduced a systematic procedure to obtain a linear representation of complex multi-terminal HVDC networks.

A. Multi-terminal HVDC networks modelling

From the viewpoint of a DC grid analysis, the multi-terminal can be represented as the interconnection of nodes and branches. An example of this representation is shown in Figure 3. The WFCs injecting power into the grid are the power input nodes and the GSCs extracting power from the grid are the power output nodes. The cables interconnecting the nodes are the branches. There are also nodes where only cables converge, those ones are called intermediate nodes. The general multi-terminal setup depicted in Figure 3 consists of m power input nodes, n power output nodes and p intermediate connection nodes and r branches. This last number depends on the particular interconnection pattern. Next, the modeling of each type of nodes is explained briefly.

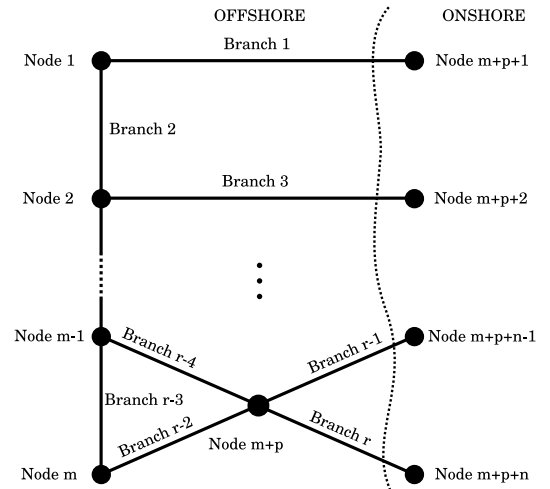


Figure 3. A node and branch scheme of a multi-terminal HVDC network

Input and output power nodes: The wind farms and the AC systems are connected to the HVDC grid through HVDC power converters. For the present analysis, it is sufficient to consider the average dynamic behavior. In this situation, the AC side of the converters are modeled as three voltage sources

and the DC side as a current source and a capacitor [18]. Using this simplified representation, each wind farm and each AC system are modeled as DC current sources, as it is illustrated in Figure 4. At the converter DC side, the power flow in the node k is represented by a current i_k coming from a source of value

$$i_k = \frac{P_k}{E_k}, \quad (2)$$

where P_k is the incoming power and E_k is the DC voltage at the node k . It will be assumed that the voltage E_k remain close to the nominal values E_0 . Under this assumption, the current i_k can be assumed proportional to the power P_k .

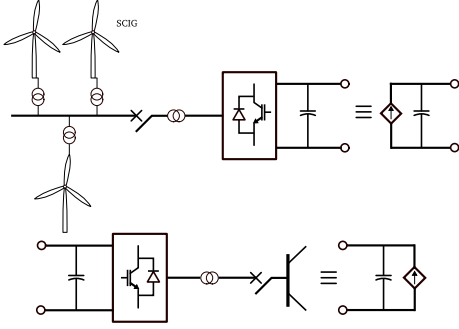


Figure 4. Equivalent representation of the wind farm and the AC grid converters for a DC grid analysis

Branches: The cables between nodes are modeled by π -equivalent circuits, see Figure 5. When these circuits converge to input or output nodes and to other π -circuits, there are several capacitors in parallel. In these circumstances, and with the aim of keeping the number of variables as minimum as possible, the total capacitances can be reduced to an equivalent one given by

$$C_k = \sum_{i=1}^l C_i. \quad (3)$$

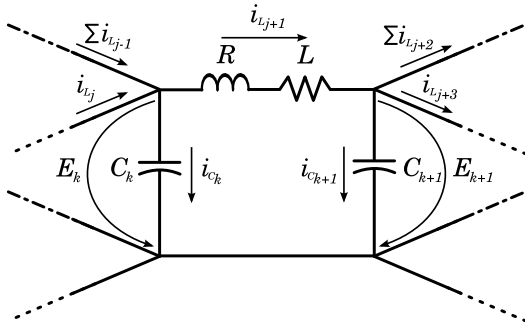


Figure 5. π -circuit modeling a branch element

Intermediate nodes: The cables in the DC grid may join two or more terminal at intermediate points. These nodes will be denoted as intermediate nodes, the node marked with $m + p$ in Figure 3 is an example of this type of nodes. Again, the number of capacitances can be reduced by replacing the capacitances of the π -equivalent circuits and the input and output nodes by a total capacitances given by (3).

An equivalent circuit can be obtained from the interconnection of the nodes and branches after the simplifications above-mentioned. Then using circuits laws and after some variable manipulations, it is possible to find a set of first order differential equations describing the dynamic behavior of the entire multi-terminal HVDC grid. These differential equations are known as the state-space representation and can be expressed in the following compact form

$$\begin{aligned} \frac{dx}{dt} &= Ax + B_w w + B_u u, \\ z &= C_z x, \\ y &= C_y x, \end{aligned} \quad (4)$$

where x is the state vector, w and u are the inputs, z and y are the outputs, and A , B_w , B_u , C_z and C_y are matrices of suitable dimensions. These matrices are obtained after arranging the variables and applying matrix computation laws.

The state vector x consists of internal variables that characterize the entire state of the system. In electrical system, the currents in the inductors and the voltages in the capacitors are commonly selected as states. Therefore, in the case of the multi-terminal HVDC network in Figure 3, the state vector is given by

$$x = [E_1, \dots, E_{m+p+n}, i_{L_1}, \dots, i_{L_r}]^T.$$

Each node has one capacitor and each branch one inductor, therefore the total number of states is $n + p + m + r$.

The inputs are divided into two vectors, the vector u gathers the variables that can be used to control the system and w are disturbances, *i.e.*, external variables that are not possible to manipulate. In the case of the multi-terminal HVDC networks, the inputs of the system are the current injected or extracted by the converters, therefore

$$\begin{aligned} w &= [i_1, \dots, i_j, \dots, i_{n_{nc}}]^T & j \in \mathcal{J}_{nc} \\ u &= [i_1, \dots, i_j, \dots, i_{n_c}]^T & j \in \mathcal{J}_c \end{aligned}$$

where \mathcal{J}_{nc} corresponds to the set of indexes of the nodes where the converters inject or extract power without voltage control and \mathcal{J}_c denotes the set of indexes of the nodes where the droop control is applied. Notice that the relation $n_c + n_{nc} = m + n$ must be held.

Similarly, the output is partitioned into two vectors. The vector y contains the variables that can be used in the control of the DC voltage. On the other hand, z stands for the vector of variables that are not available to be used by the controller. In the multi-terminal HVDC scheme, the controllers can only use the information provided by the voltage at the nodes where droop control is applied. The rest of the voltages must also be maintained close to the rated values but they cannot be fed back to the controllers. Hence,

$$\begin{aligned} z &= [E_1, \dots, E_j, \dots, E_{n_{nc}}]^T & j \in \mathcal{J}_{nc} \\ y &= [E_1, \dots, E_j, \dots, E_{n_c}]^T & j \in \mathcal{J}_c \end{aligned}$$

The transfer matrix of the system

$$G(s) = \begin{bmatrix} G_{zw}(s) & G_{zu}(s) \\ G_{yw}(s) & G_{yu}(s) \end{bmatrix} \quad (5)$$

is obtained from the state-space equation (4), where

$$\begin{aligned} G_{zw}(s) &= C_z(sI - A)^{-1}B_w, \\ G_{zu}(s) &= C_z(sI - A)^{-1}B_u, \\ G_{yw}(s) &= C_y(sI - A)^{-1}B_w, \\ G_{yu}(s) &= C_y(sI - A)^{-1}B_u. \end{aligned}$$

The transfer matrices G_{zu} and G_{yu} relate the currents imposed by the controller with the controlled and non directly controlled voltages, respectively. Whereas, the transfer matrices G_{zw} and G_{yw} connect the current not used in the control with the controlled and non directly controlled voltages, respectively.

B. Droop gain selection

In a multi-terminal scheme, the distance among converts is usually large and the communications are not reliable enough to be used in the DC voltage control. As consequence, each controller must compute the control variables from the information provided by the voltage at the own node. In matrix terms, the multi-variable controller has an expression of the form

$$K = \begin{bmatrix} K_G \cdot q_1 & & 0 \\ & \ddots & \\ 0 & & K_G \cdot q_{n_c} \end{bmatrix} = K_G \begin{bmatrix} q_1 & & 0 \\ & \ddots & \\ 0 & & q_{n_c} \end{bmatrix} \quad (6)$$

where K_G is a scalar parameter to be determined and q_j are the n_c constants obtained from a steady-state study [17]. These constants are associated with the resistance values of the line and the amount of power incoming or outgoing from each terminal. These constants are positive in the case of power output nodes and negative in the case of power input nodes.

The droop control scheme is depicted in Figure 6. It can be observed that only the variable y is fed back into the controller K . The objective of the droop control is to maintain the DC voltage within desired limits when the system is disturbed by the varying currents of the nodes without voltage control. The control input also must be kept under the limits imposed by the maximum currents in the converters. Therefore, the selection of the gain K_G must take into account these performance specifications besides guaranteeing closed loop stability. From Figure 6, it is easy to prove that the variables of interest are given by the following expressions

$$e(s) = y(s) - E_0(s) = [S(s)G_{yw}(s) \quad -S(s)]v(s), \quad (7)$$

$$z(s) = [(G_{zw}(s) + G_{zu}(s)KS(s)G_{yw}(s)) \\ -G_{zu}(s)KS(s)]v(s), \quad (8)$$

$$u(s) = [KS(s)G_{yw}(s) \quad -KS(s)]v(s). \quad (9)$$

where $v(s) = [w(s) \ E_0(s)]^T$, $S(s) = (I_{n_c} - G_{yu}(s)K)^{-1}$ is the sensitivity transfer function with I_{n_c} the identity matrix of dimension $n_c \times n_c$.

The effect of the gain K_G on the stability can be analyzed by computing the eigenvalues of the closed loop matrix A_{cl} . Replacing $u = K(y - E_0)$ in the state-space equations (4), the closed loop matrix is given by $A_{cl} = A + K_G B_u C_y$. Then, for closed loop stability, the gain K_G must ensure that all

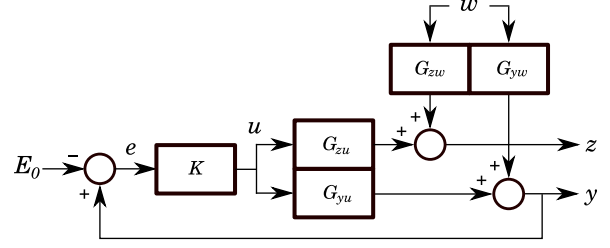


Figure 6. Droop control scheme in a multi-terminal grid

eigenvalues of A_{cl} have negative real part. A simple power analysis reveals that the closed loop system is stable for any $K_G > 0$. In fact, since the control law makes the current i_k (with $k \in \mathcal{J}_c$) proportional to the voltage E_k at the same node, the gain $K_G q_k$ can be interpreted as an passive admittance. That is, the droop control is similar to add energy dissipation to the system and therefore the closed loop system will be always stable for $K_G > 0$.

The relation between the gain K_G and the performance objectives can be analyzed with the help of the frequency response of the system. This analysis consists in evaluating the transfer function in $s = j\omega$ and in analyzing the singular values of the resultant complex matrix functions of $j\omega$. The singular values of the frequency response of $G(s)$ is denoted as

$$\sigma_i(G(j\omega)) = \lambda_i(G(j\omega)^T G(j\omega))$$

where $\lambda_i(\cdot)$ denotes the i -th eigenvalue of the matrix. The singular values provide information about how a vector of sinusoidal signals of frequency ω is altered by the system. In multi-input multi-output linear systems, a vector of sinusoidal signals suffers not only a change in its magnitude and phase, but also a change in its direction. The maximum amplification that the vector can experience is given by the maximum singular value $\bar{\sigma}(G(j\omega))$ and the minimum amplification by the minimum singular value $\underline{\sigma}(G(j\omega))$. This analysis can be interpreted as the extension of the popular single-input single-output frequency response analysis to multi-variable systems. Here, the magnitude of the frequency response is replaced by the singular values (see [19] for a more detailed explanation).

The performance specifications are to minimize the effect of the disturbances on the DC voltages and to maintain the control input under reasonable limits. These specifications can be expressed in terms of the singular values in order to determine the constraints on K_G . For example, the maximum energy of the error caused by any input v of bounded energy is given by

$$\max_{v \neq 0} \frac{\|e\|_2}{\|v\|_2} = \max_{\omega} \bar{\sigma}(T_{ev}(j\omega)),$$

where $\|e\|_2^2 = \int e^T e dt$ denotes the 2-norm of e . Therefore, to minimize the effects of the disturbance v on the voltage error

Table I
PARAMETER OF THE FOUR-TERMINAL EXAMPLE

Grid parameters	Value
Line resistance R_1	0.50 Ω
Line resistance R_2	0.25 Ω
Line resistance R_3	0.40 Ω
Line inductance L_1	5.0 mH
Line inductance L_2	2.5 mH
Line inductance L_3	4.0 mH
Capacitances C_k ($k = 1, \dots, 4$)	150 μ F
Rated line current i_L^{rtd}	667 A
Rated input current i_k^{rtd}	667 A
Converter rated power P_k	100 MW
Rated DC voltage E_k	150 kV
Reference voltage E_0	145 kV

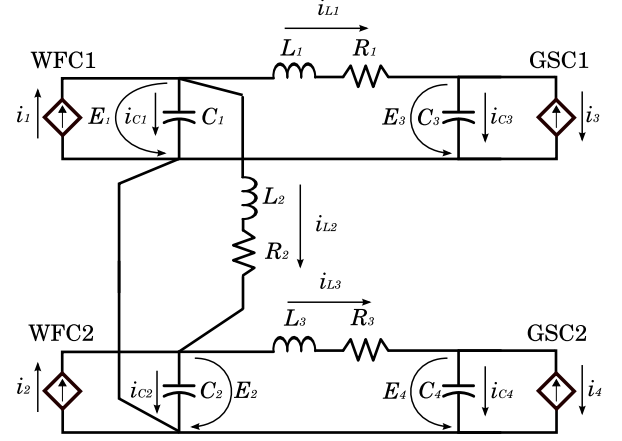


Figure 7. Four-terminal grid used to illustrate the droop constant selection methodology

e and on z can be interpreted as minimizing

$$\bar{\sigma} \left(\begin{bmatrix} S(j\omega)G_{yw}(j\omega) & -S(j\omega) \\ (G_{zw}(j\omega) + G_{zu}(j\omega)KS(j\omega))G_{yw}(j\omega) & -G_{zu}(j\omega)KS(j\omega) \end{bmatrix} \right)$$

and to maintain the control input under reasonable limits can be expressed as ensuring that

$$\bar{\sigma} \left(\begin{bmatrix} KS(j\omega)G_{yw}(j\omega) & -KS(j\omega) \end{bmatrix} \right)$$

is bounded in the frequencies of interest.

In general, large values of K_G achieves a smaller voltage error but may also demand large control inputs. The optimal K_G is a compromise among all these objectives.

IV. FOUR-TERMINAL GRID EXAMPLE

A simple four-terminal HVDC grid is used to illustrate the droop selection methodology presented in previous sections. The four-terminal grid is depicted in Figure 7 and consists of two offshore wind farm converters WFC1 and WFC2 and two onshore grid side converters GSC1 and GSC2. The values of the parameters are listed in Table I. The four-terminal HVDC grid has two power input nodes, two power output nodes and three branches representing the cables linking the converters. The capacitors are the result of combining the capacitances of the nodes and the corresponding branch side, as explained in Section III-A.

Two scenario are analyzed. In the first case, droop control is applied in both grid side converters whereas the wind farm converters inject all the wind power available. In the second scenario, due to a fault in the AC grid, both wind farm converters regulate the DC voltages and the grid side converters extract power from the HVDC grid at their maximum capacity.

A. Case 1: Droop control in the AC grid side

Applying circuit laws to the four-terminal grid in Figure 7, the following differential equations can be obtained

$$\frac{dE_1}{dt} = \frac{1}{C_1}i_{C_1}, \quad \frac{dE_2}{dt} = \frac{1}{C_2}i_{C_2}, \quad (10)$$

$$\frac{dE_3}{dt} = \frac{1}{C_3}i_{C_3}, \quad \frac{dE_4}{dt} = \frac{1}{C_4}i_{C_4}, \quad (11)$$

$$\frac{di_{L_1}}{dt} = \frac{1}{L_1}(-R_1 i_{L_1} + E_1 - E_3), \quad (12)$$

$$\frac{di_{L_2}}{dt} = \frac{1}{L_2}(-R_2 i_{L_2} + E_1 - E_2), \quad (13)$$

$$\frac{di_{L_3}}{dt} = \frac{1}{L_3}(-R_3 i_{L_3} + E_2 - E_4), \quad (14)$$

and the following algebraic equations

$$i_{C_1} = i_1 - i_{L_1} - i_{L_2}, \quad (15)$$

$$i_{C_2} = i_2 - i_{L_3} - i_{L_2}, \quad (16)$$

$$i_{C_3} = -i_3 + i_{L_1}, \quad (17)$$

$$i_{C_4} = -i_4 + i_{L_3}. \quad (18)$$

There are four capacitors and three inductor; therefore, the variables $E_1, E_2, E_3, E_4, i_{L_1}, i_{L_2}$ and i_{L_3} are sufficient to completely define the state of this system, *i.e.*,

$$x = [E_1 \ E_2 \ E_3 \ E_4 \ i_{L_1} \ i_{L_2} \ i_{L_3}]^T.$$

As the WFCs are injecting all available power into the grid and in the GSCs are regulating the DC voltages, the input and output result divided into

$$\begin{aligned} w &= [i_1 \ i_2]^T, & u &= [i_3 \ i_4]^T, \\ z &= [E_1 \ E_2]^T, & y &= [E_3 \ E_4]^T. \end{aligned}$$

The purpose of the droop control applied on the right side of the four-terminal grid in Figure 7 is to maintain the DC voltage stable when the currents coming from the wind farm converters WFC1 and WFC2 change. Therefore, the vector of these currents is the disturbance w and the control input u is the vector of the currents of the GSCs i_3 and i_4 . The voltages measured and fed back to the controller are the voltages E_3

and E_4 whereas the voltages E_1 and E_2 are not available for the controller but it is desirable to maintain them close to the rated value.

After the previous definitions, substituting the currents in the capacitors in (10)–(11) by the relations (15)–(18) and reorganizing the differential equations, the matrices in the state-space representation (4) result

$$A = \begin{bmatrix} 0 & 0 & 0 & 0 & -\frac{1}{C_1} & -\frac{1}{C_1} & 0 \\ 0 & 0 & 0 & 0 & 0 & -\frac{1}{C_2} & -\frac{1}{C_2} \\ 0 & 0 & 0 & 0 & -\frac{1}{C_3} & 0 & 0 \\ 0 & 0 & 0 & 0 & 0 & 0 & -\frac{1}{C_4} \\ \frac{1}{L_1} & 0 & -\frac{1}{L_1} & 0 & -\frac{R_1}{L_1} & 0 & 0 \\ \frac{1}{L_2} & -\frac{1}{L_2} & 0 & 0 & 0 & -\frac{R_2}{L_2} & 0 \\ 0 & \frac{1}{L_3} & -\frac{1}{L_3} & 0 & 0 & 0 & -\frac{R_3}{L_3} \end{bmatrix},$$

$$B_w = \begin{bmatrix} \frac{1}{C_1} & 0 \\ 0 & \frac{1}{C_2} \\ 0 & 0 \\ 0 & 0 \\ 0 & 0 \\ 0 & 0 \\ 0 & 0 \end{bmatrix}, \quad B_u = \begin{bmatrix} 0 & 0 \\ 0 & 0 \\ -\frac{1}{C_3} & 0 \\ 0 & -\frac{1}{C_4} \\ 0 & 0 \\ 0 & 0 \\ 0 & 0 \end{bmatrix},$$

$$C_z = \begin{bmatrix} 1 & 0 & 0 & 0 & 0 & 0 & 0 \\ 0 & 1 & 0 & 0 & 0 & 0 & 0 \end{bmatrix},$$

$$C_y = \begin{bmatrix} 0 & 0 & 1 & 0 & 0 & 0 & 0 \\ 0 & 0 & 0 & 1 & 0 & 0 & 0 \end{bmatrix}$$

The droop controller in the case of two inputs and two outputs is simply

$$K = K_G \cdot \begin{bmatrix} 1 & 0 \\ 0 & 1 \end{bmatrix} = K_G \cdot I_2$$

The constants q_1 and q_2 have been set in 1 because all the lines are of the same longitude and it is desired to extract the same amount of power from each terminal.

In Figure 8, it can be found the eigenvalues of the close loop matrix A_{cl} for several values of gain K_G . Notice that the real parts of the eigenvalues become more negative for higher values of gain. This stabilizing effect is in accordance with the fact that an increment in the droop constant is similar to incrementing the energy dissipation in the system.

As mentioned in Section III-B, the droop constant is selected in accordance with a performance criterion measured in terms of the 2-norm of the voltage error e , of the voltage not measured z and of the control input u .

The voltage error is given by (7), where we are interested in the particular input $E_0 = [145 \text{ kV } 145 \text{ kV}]^T$. In this situation, the transfer $S(s)$ have a transmission zero at $s = 0$ for the particular direction of E_0 , e.g., for $K_G = 1$

$$S(0) = \begin{bmatrix} -0.32 & 0.32 \\ 0.32 & -0.32 \end{bmatrix} \cdot \begin{bmatrix} 145 \text{ kV} \\ 145 \text{ kV} \end{bmatrix} = \begin{bmatrix} 0 \\ 0 \end{bmatrix},$$

this also holds for any other value of K_G . As consequence, the voltage error reduces to

$$e(s) = S(s)G_{yw}(s)w(s). \quad (19)$$

The singular values of $S(s)G_{yw}(s)$ can be seen in Figure 9, it is clear that the larger the K_G the smaller the error. In

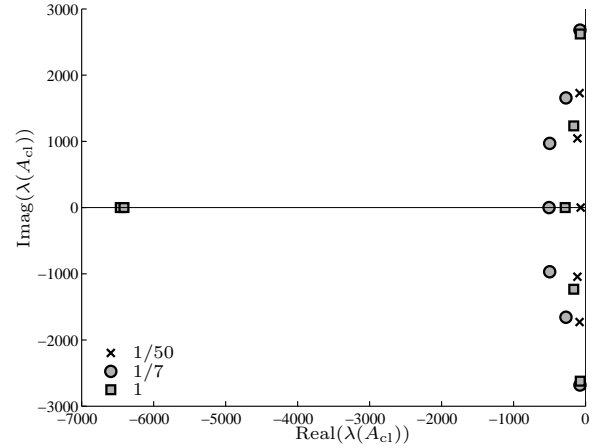


Figure 8. Eigenvalues of the closed loop matrix A_{cl} for several values of K_G (Case 1)

particular, at $s = 0$ and for the maximum voltage error of 10% ($e_{\max} = \pm 15 \text{ kV}$) and the rated current $i_{\text{rtid}} = 667 \text{ A}$,

$$\bar{\sigma}(S(0)G_{yw}(0)) \leq \frac{\|e(0)\|_2}{\|w(0)\|_2} = \frac{\sqrt{15000^2 + 15000^2}}{\sqrt{667^2 + 667^2}} = 22.5.$$

This constraint can be extended to the rest of the frequencies resulting in the shadow area in Figure 9. The constraint on the error is relaxed in high frequencies since it is impossible to satisfy a uniform limit without violating the bandwidth limitations of the converters. The transfer functions $S(s)G_{yw}(s)$ which their singular values are inside the shadow area in Figure 9 satisfy the error constraints. In a case of 2×2 transfer matrix it is not possible to find that

$$\bar{\sigma}(S(0)G_{yw}(0)) = \frac{1}{K_G}$$

therefore, $K_G \geq 1/22.5$. In more general cases, the limit on the gain K_G can be found numerically.

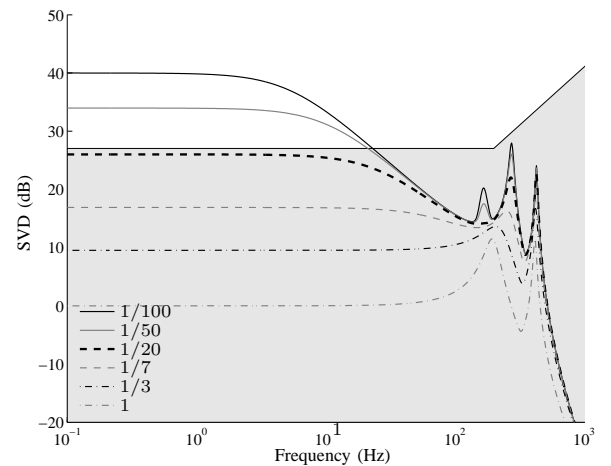


Figure 9. The maximum singular values of the function $S(s)G_{yw}(s)$ for several values of K_G (Case 1). The singular values inside the shadow area satisfy the error constraint

The effect of K_G on the output z is given by (8). The objective is to maintain the DC voltage in the non directly

controlled terminal voltage close to a rated value. Again, the particular input $E_0 = [145 \text{ kV } 145 \text{ kV}]^T$ is considered. For this particular input, the output of $G_{zu}(s)KS(s)$ is independent of K_G and results equal to the input, *i.e.*,

$$G_{zu}(0)KS(0) \cdot \begin{bmatrix} 145 \text{ kV} \\ 145 \text{ kV} \end{bmatrix} = \begin{bmatrix} 145 \text{ kV} \\ 145 \text{ kV} \end{bmatrix}.$$

Therefore, it is possible to analyze the deviation from the rated value by defining $e_z = z - E_0$,

$$e_z(s) = (G_{zw}(s) + G_{zu}(s)KS(s)G_{yw}(s))w(s).$$

Figure 10 show the singular values of this transfer function. It can be observed that for higher values of K_G the maximum singular values of $G_{zw}(s) + G_{zu}(s)KS(s)G_{yw}(s)$ becomes smaller in low frequencies. However, in high frequencies, as Figure 10 shows, an increment of K_G may produce the opposite effect in certain cases. It can be seen that for $K_G \geq 1/20$ the singular values are inside the shadow area and fulfilled the constraints on the variable e_z . In particular, at $s = 0$ and $K_G = 1/22.5$, the voltage in the wind farm nodes result

$$e_z(0) = \begin{bmatrix} 11.54 & 11.41 \\ 11.41 & 11.54 \end{bmatrix} \cdot \begin{bmatrix} 667 \text{ A} \\ 667 \text{ A} \end{bmatrix} = \begin{bmatrix} 15.3 \text{ kV} \\ 15.3 \text{ kV} \end{bmatrix}$$

that is, a 10% of error in the voltage.

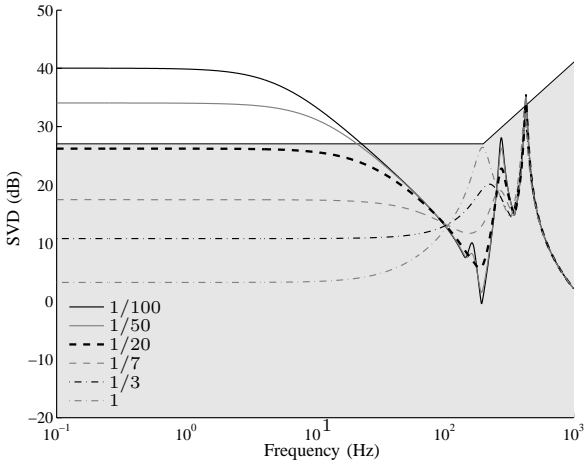


Figure 10. The maximum singular values of the function $G_{zw}(s) + G_{zu}(s)KS(s)G_{yw}(s)$ for several values of K_G (Case 1). The singular values inside the shadow area satisfy the constraint on e_z .

The control input is given by (9). Again, as we are interested in the particular input $E_0 = [145 \text{ kV } 145 \text{ kV}]^T$, this signal results governed by the transfer $KS(s)G_{yw}(s)$. Figure 11 shows the maximum singular values of $KS(s)G_{yw}(s)$ for several values of K_G . The shadow area indicates the singular values that satisfy the performance specifications. Notice that the constraint decreases in high frequencies to consider the limits on the bandwidth of the converters. It can be observed that the low frequency components of the control input are independent of the value of K_G . However, in high frequencies this transfer presents resonance peaks that for some values of K_G violate the constraints indicated by the shadow area. This constraint imposes an upper limit on the gain K_G . In particular,

from Figure 11 it can be concluded that $K_G \leq 1/20$ to fulfil the constraint on the control input.

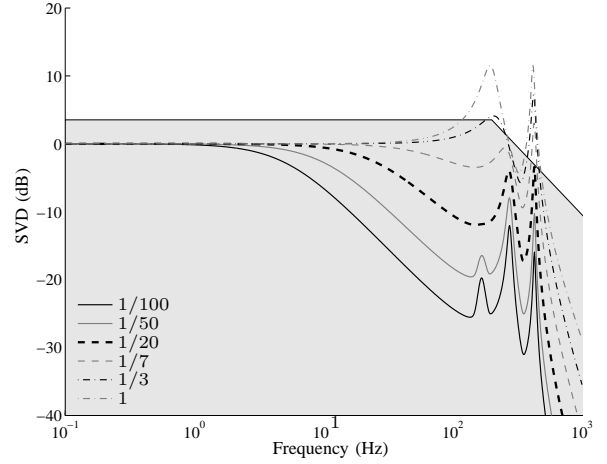


Figure 11. The maximum singular values of the function $KS(s)G_{yw}(s)$ for several values of K_G (Case 1). The singular values inside the shadow area satisfy the constraint on the control input.

From the previous analysis, it can be concluded that the gain K_G that better suits the performance specifications is $1/20$.

In order to evaluate the droop gain previously selected, simulations were carried out in Matlab-Simulink. The analyzed scenario corresponds to two simultaneous and equal changes in the power injected into the DC grid by the WFCs. The powers injected by the two converters change from 0 MW to the rated value at 0.05 s and return to 0 MW at 0.20 s. Figure 12a shows the power flow at each converter. The solid lines correspond to the power injected by the WFCs and the dashed lines to the power extracted by the GSCs. It can be observed that the power ongoing from the GSCs are almost coincident due to the selection of the power distribution factors $q_1 = q_2 = 1$. As consequence, both GSCs extract approximately the same amount of power. The power losses of the DC grid, at rated power transmission, are around 375 kW. The evolution of the terminal voltages can be seen in Figure 12b. The DC voltages remain at 145 kV during the period where the power flow is zero since there is no voltage drop in the grid resistances. Once the power input increases, the DC voltages move toward a new voltage equilibrium. Notice that during nonzero power flow, there are differences between the voltage at the wind farm terminals and the voltages in the grid side terminals due to the power flow direction. Figure 12c shows the currents flowing through each VSCs. Both power and current evolutions are similar, except for a scale factor, which indicates that the initial approximation of considering the current proportional to the power has been reasonable. It can also be observed that the currents never exceed the converter limits.

B. Case 2: Droop control in the wind farm side

In the second case of study, it is assumed that a simultaneous fault in both AC grids forces the GSCs to enter in current limitation mode. In this circumstance, the WFCs are responsible for regulating the DC voltage. Hence, the control inputs are

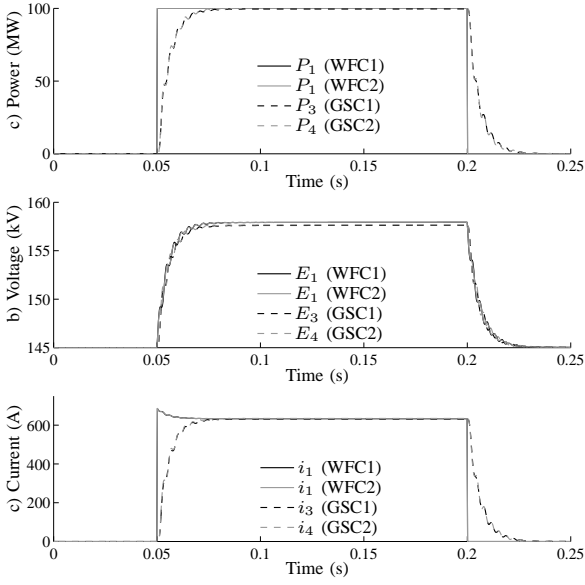


Figure 12. Simulations corresponding to a change in the power injected into the grid by the wind farm converters (Case 1)

the currents injected by the WFCs and the disturbances are the currents extracted by the GSCs, *i.e.*

$$w = [i_3 \ i_4]^T, \quad u = [i_1 \ i_2]^T.$$

On the other hand, the measured variables are the wind farm side voltages and the non-directly controlled variables are the grid side voltages, *i.e.*

$$z = [E_1 \ E_2]^T, \quad y = [E_3 \ E_4]^T.$$

The state space model have the same matrix A but the input and output matrices are now given by

$$B_w = \begin{bmatrix} 0 & 0 \\ 0 & 0 \\ -\frac{1}{C_3} & 0 \\ 0 & -\frac{1}{C_4} \\ 0 & 0 \\ 0 & 0 \\ 0 & 0 \end{bmatrix}, \quad B_u = \begin{bmatrix} \frac{1}{C_1} & 0 \\ 0 & \frac{1}{C_2} \\ 0 & 0 \\ 0 & 0 \\ 0 & 0 \\ 0 & 0 \\ 0 & 0 \end{bmatrix},$$

$$C_z = \begin{bmatrix} 0 & 0 & 1 & 0 & 0 & 0 & 0 \\ 0 & 0 & 0 & 1 & 0 & 0 & 0 \end{bmatrix},$$

$$C_y = \begin{bmatrix} 1 & 0 & 0 & 0 & 0 & 0 & 0 \\ 0 & 1 & 0 & 0 & 0 & 0 & 0 \end{bmatrix}.$$

The droop controller in the case is

$$K = K_G \cdot \begin{bmatrix} -1 & 0 \\ 0 & -1 \end{bmatrix} = -K_G \cdot I_2,$$

since the droop control is applied in the wind farm side.

Figure 13 shows the eigenvalues of the close loop matrix A_{cl} for several values of gain K_G . Notice that the real parts of the eigenvalues become more negative for higher values of gain.

Also in this scenario, it is considered the case where $E_0 = [145 \text{ kV} \ 145 \text{ kV}]^T$. Therefore, the performance is associated

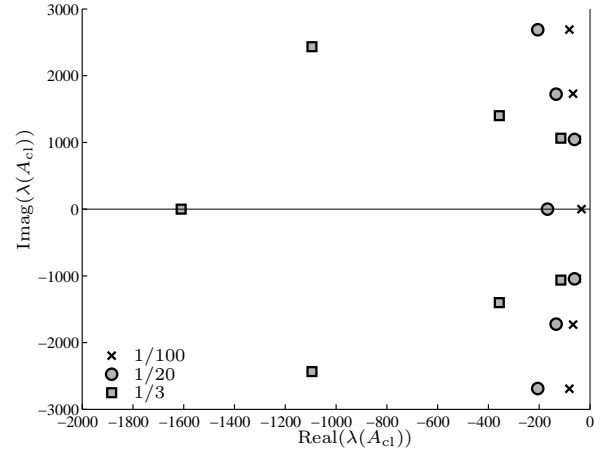


Figure 13. Eigenvalue of the closed loop matrix A_{cl} for several values of K_G (Case 2)

only with the input $w(s)$. In Figures 14-15, it can be seen the maximum singular values of the transfers $S(s)G_{yw}(s)$, $G_{zw}(s) + G_{zw}(s)KS(s)G_{yw}(s)$ and $G_{zu}(s)KS(s)$ for several values of K_G . The resonance peaks are lighter damped in this case. For this reason, in order to fulfil the low frequencies error, larger values must be accepted in high frequencies. Notice in Figure 16 that the constraint on the control input has been relaxed in high frequency for the same reason. As consequence, the gain K_G has been set at $1/20$.

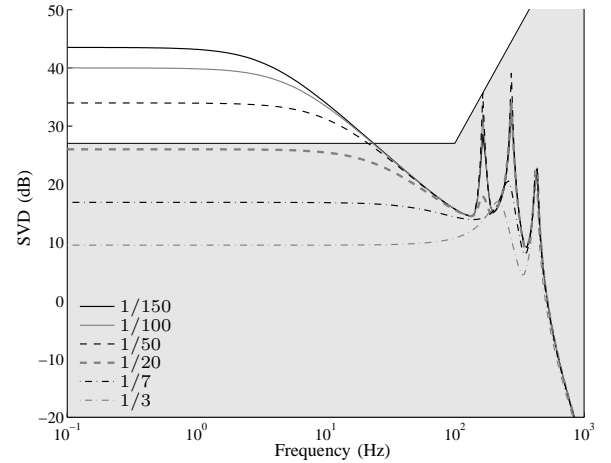


Figure 14. The maximum singular values of the function $S(s)G_{yw}(s)$ for several values of K_G (Case 2). The singular values inside the shadow area satisfy the error constraint

The system has been also evaluated by simulations. In the scenario considered, both WFCs inject the rated power value while two voltage sags are applied in the AC grid. A three phase voltage sag of 10% of the nominal AC values is applied to the AC grid connected to the GSC1. At the same time, another voltage sag of 20% is applied to the grid connected to the GSC2. The both sags last 0.2 s. The three phase voltages at each AC grid are shown in Figure 17 whereas the corresponding three phase currents can be seen in Figure 18.

Figure 19 presents the evolution of the variables in the

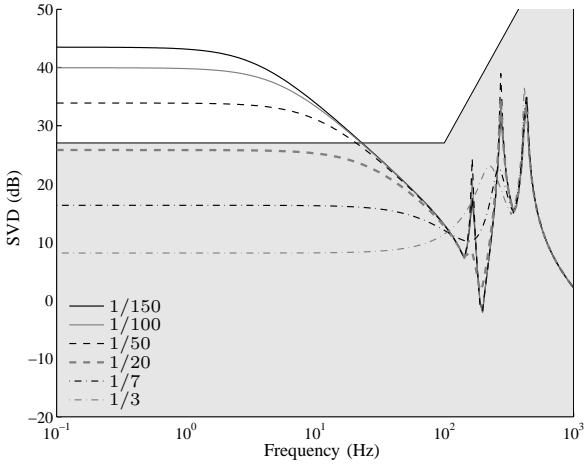


Figure 15. The maximum singular values of the function $G_{zw}(s) + G_{zw}(s)KS(s)G_{yw}(s)$ for several values of K_G (Case 2). The singular values inside the shadow area satisfy the constraint on e_z

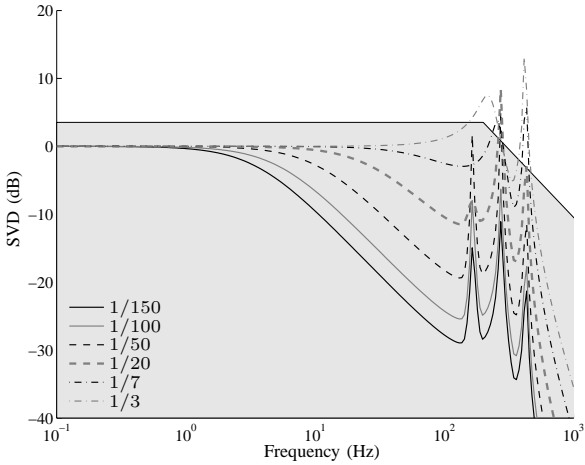


Figure 16. The maximum singular values of the function $KS(s)G_{yw}(s)$ for several values of K_G (Case 2). The singular values inside the shadow area satisfy the constraint on the control input

DC grid. It can be observed that the AC grid fault provokes an increment of the all DC voltages (Figure 19b). These increments are due to the fact that the GSCs operate in current limitation mode to avoid the disconnection by over-currents during the grid fault. When the WFCs voltages exceed 160 kV, the corresponding converters start to applied droop control in the DC grid, reducing the power injected to the grid from 100 MW to 20 MW. (Figure 19a). The DC voltage limit is 164.5 kV. The DC current also decreases during the voltage sag due to the power reduction caused by the droop control in the WFCs (Figure 19c). Notice that the disconnection of the system due to over-voltage was avoided during the fault.

V. CONCLUSIONS

A design methodology for droop control in multi-terminal HVDC grids has been presented. The methodology includes a systematic procedure to formulate a linear model of the multi-terminal grids. Based on this model and a frequency

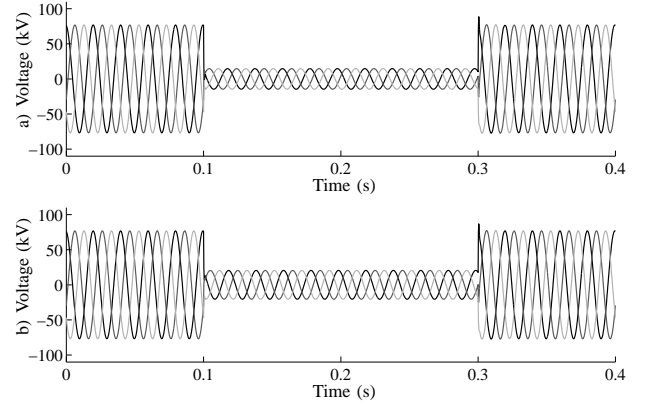


Figure 17. Simulations corresponding to a voltage sag in the AC grids (Case 2). a) Three phase voltages in the grid 1, b) three phase voltages in the grid 2

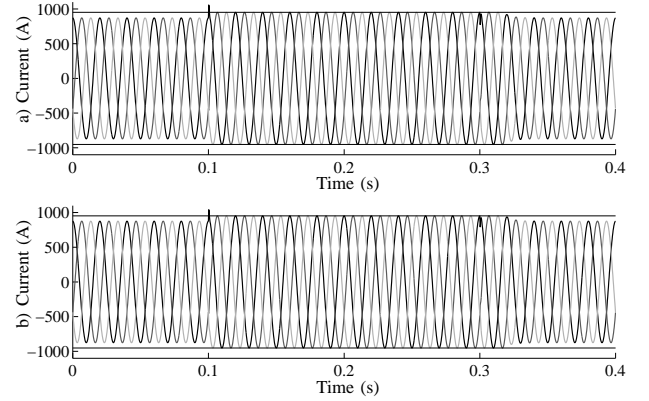


Figure 18. Simulations corresponding to a voltage sag in the AC grids (Case 2). a) Three phase currents in the grid 1, b) three phase currents in the grid 2

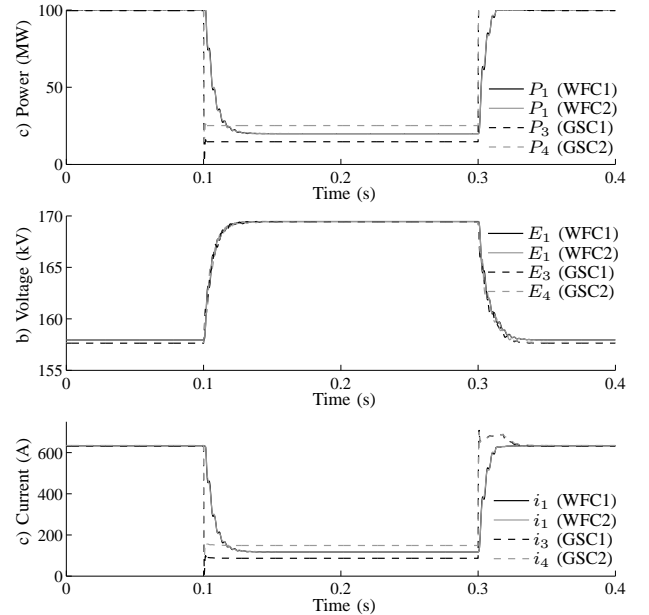


Figure 19. Simulations corresponding to a voltage sag in the AC grids (Case 2)

response analysis, it is provided a criterion to select the droop gain taking into account the dynamics of the entire multi-terminal HVDC system. The limitation of DC voltage errors and the converter currents defines a range on the droop gains that achieve the better compromise between the specifications. Each local controller can affect the global stability and the DC voltage in other terminals. For these reasons, the droop constant selection must be addressed in the context of multi-variable system theory to consider the dynamic behavior of the entire multi-terminal grid, both in normal operation and in fault conditions.

A four-terminal grid example has been used to illustrate the application of the use of the methodology. Nevertheless, the procedure is applicable to any other multi-terminal HVDC grids with more inputs and outputs. The complexity of the model increases with the number of nodes and branches but the computation of the singular values does not involve a serious limitation with the current algorithms. The range of droop gains is obtained only from the maximum singular values; therefore, its computation is independent of the complexity of the particular multi-terminal grid.

REFERENCES

- [1] T. Ackermann. Transmission systems for offshore wind farms. *IEEE Power Engineering Review*, 22(12):23–27, Dec. 2002.
- [2] J. Reeve. Multiterminal HVDC power systems. *IEEE Transactions on Power Apparatus and Systems*, PAS 99(2):729–737, 1980.
- [3] J. Arrillaga. *High Voltage Direct Current Transmission*. Institution of Electrical Engineers, London, U.K., 2nd edition, 1998.
- [4] U. Axelsson, A. Holm, C. Liljegren, M. Aberg, K. Eriksson, and O. Tollerz. The Gotland HVDC light project-experiences from trial and commercial operation. In *Proc. of the 16th Int. Conf. and Exhibition on Contributions Electricity Distribution CIRED.*, volume 1, page 5pp., 18–21 June 2001.
- [5] J. Dorn, H. Huang, and D. Retzmann. A new multilevel voltage-sourced converter topology for HVDC applications. In *Proc. of the Cigré Session 2008. B4 HVDC and Power Electronics*, 2008.
- [6] O. Gomis-Bellmunt, J. Liang, J. Ekanayake, R. King, and N. Jenkins. Topologies of multiterminal HVDC-VSC transmission for large offshore wind farms. *Electrical Power Systems Research*, 81(2):271–281, 2011.
- [7] O. Gomis-Bellmunt, J. Liang, J. Ekanayake, and N. Jenkins. Voltage-current characteristics of multiterminal HVDC-VSC for offshore wind farms. *Electrical Power Systems Research*, 81(2):440–450, 2011.
- [8] ABB. Grid connection of offshore wind farms - BorWin1. www.abb.com/hvdc, 2010.
- [9] J. Liang, O. Gomis-Bellmunt, J. Ekanayake, and N. Jenkins. Control of multi-terminal VSC-HVDC transmission for offshore wind power. In *Proc. of the 13th European Conf. Power Electronics and Applications (EPE '09)*, pages 1–10, 2009.
- [10] E. Uhlmann U. Lamm and P. Danfors. Some aspects of tapping HVDC transmission systems. *Direct Current*, 8(5):124–129, 1963.
- [11] J. Reeve and J. Arrillaga. Series connection of converter stations in an HVDC transmission system. *Direct Current*, 10(2):72–78, 1965.
- [12] W. Lu and B.T. Ooi. Optimal acquisition and aggregation of offshore wind power by multiterminal voltage source HVDC. *IEEE Transactions on Power Delivery*, 18(1):201–206, 2003.
- [13] Desertec Foundation. Red paper. an overview of the desertec concept. www.desertec.com, 2010.
- [14] Airtricity. European offshore supergrid proposal. www.airtricity.com, 2010.
- [15] P. Kundur. *Power System Stability and Control*. McGraw-Hill Professional, 1994.
- [16] J. Machowski, J. Bialek, and J. Bumby. *Power system dynamics and stability*. Wiley, 1997.
- [17] L. Xu, L. Yao, and M. Bazargan. DC grid management of a multi-terminal HVDC transmission system for large offshore wind farms. In *Proc. of the Int. Conf. Sustainable Power Generation and Supply (SUPERGEN '09)*, pages 1–7, 2009.
- [18] G. Zhang, Z. Xu, and Y. Cai. An equivalent model for simulating VSC based HVDC. In *Proc. of the IEEE/PES Transmission and Distribution Conf. and Exposition*, volume 1, pages 20–24, 2001.
- [19] S. Skogestad and I. Postlethwaite. *Multivariable Feedback Control, Analysis and Design*. John Wiley & Sons, Ltd, 2007.



Eduardo Prieto-Araujo was born in Barcelona, Spain, in 1986. He received the degree in Industrial Engineering from the Universitat Politècnica de Catalunya, Barcelona (UPC), Spain, in 2011. His area of interest are the modeling and control of electrical machines, power converters and HVDC grids, related with renewable generation systems.



Fernando D. Bianchi received the B.S. and the Ph.D. degrees in Electronic Engineering from the National University of La Plata (UNLP), Argentina, in 1999 and in 2005, respectively. From 1999 to 2006, he was a Ph.D. student and a postdoctoral fellow at the Laboratory of Industrial Electronic, Control and Instrumentation (LEICI, UNLP, Argentina). From 2006 to 2010, he was a postdoctoral researcher at Technical University of Catalonia (UPC), Spain. In 2010, he joined the Power Electronics and Electric Power Grids Group at Catalonia Institute for Energy Research (IREC) as a scientific researcher. His main research interests include robust control and linear parameter varying (LPV) systems and their applications to the control of renewable energy conversion systems.



Adrià Junyent-Ferré was born in Barcelona, Spain, in 1982. He received the degree in industrial engineering from the Universitat Politècnica de Catalunya, Barcelona (UPC), Spain, in 2007. He is currently pursuing PhD in Electrical Engineering in the Department of Electrical Engineering of the UPC since 2007. His area of interest is the control of power electronic converters for the operation of renewable generation systems under different grid fault conditions.



Oriol Gomis-Bellmunt (S'05-M'07) received the degree in industrial engineering from the School of Industrial Engineering of Barcelona (ETSEIB), Technical University of Catalonia (UPC), Barcelona, Spain, in 2001 and the PhD in electrical engineering from the UPC in 2007. In 1999 he joined Engitrol S.L. where he worked as project engineer in the automation and control industry. In 2003 he developed part of his PhD thesis in the DLR (German Aerospace center) in Braunschweig (Germany). Since 2004 he is with the Electrical Engineering

Department of the UPC where he is lecturer and participates in the CITCEA-UPC research group. Since 2009 he is also with the Catalonia Institute for Energy Research (IREC). His research interests include the fields linked with smart actuators, electrical machines, power electronics, renewable energy integration in power systems, industrial automation and engineering education.